Supporting Information

Constructing Fe-N-doped porous carbon nanofiber for pH-universal ORR and switchable superior Zn-air batteries

Yu Ma[1,2], Yuhan Xiao[1], Yanfeng Ge[1], Degong Gao[3], Yunge Zhang[1], Zepeng Li[1] and Yingdong Han[1,2*]*

[1] *College of Science, Civil Aviation University of China, Tianjin, P. R. China*

[2] *Institute of Environment and Sustainable Development, Civil Aviation University of China, Tianjin, P. R. China*

[3] *Shandong Daisheng Construction Co., Ltd, Taian, P. R. China*

[*]Corresponding author:
E-mail: hansuo@126.com (Y. Han)

E-mail: li_zepeng@163.com (Z. Li)

Experimental Section

Chemical reagents and raw materials: Bacterial cellulose (BC) dispersion was kindly provided by Hainan Yeguo Foods Co., Ltd., Hainan, China. $FeCl_3 \cdot 6H_2O$, $Zn(NO_3)_2 \cdot 6H_2O$, 2-methylimidazole (2-MIM) and tert-butyl alcohol (TBA) were purchased from Aladdin and directly used without further purification. The commercial Pt/C catalyst (20 wt%), 0.1 M phosphate buffered saline (PBS, pH 7.4) and Nafion solution (5 wt%) were acquired from Sigma-Aldrich. All the water used in the present study was deionized water.

Preparation of Fe(Zn)-N-C: Bacterial cellulose nanofibers were chemical treatments via an improved 2,2,6,6-tetramethylpiperidine-1-oxyl radical (TEMPO) method according to our previous work[1]. The TEMPO-mediated cellulose nanofibers were named as TOBC. The $Zn(NO_3)_2 \cdot 6H_2O$ (86 mg) was mixed with a suspension of ion-exchanged TOBC (25 mL BC) immediately. Then mixtures were washed by deionized water five times. The product was poured into 25 mL of 5:1 (v:v) water/TBA mixture, followed by stirring at room temperature (R.T.) for 2 h. The aqueous suspension was added into $FeCl_3 \cdot 6H_2O$ (50 mg), $Zn(NO_3)_2 \cdot 6H_2O$ (255.8 mg) and 2-MIM (2824.6 mg) together and followed by stirring for 15 minutes, then through centrifugation, repetitive rinsing by deionized water and freeze-drying for 48 h. Finally, the mixture was pyrolyzed in Ar atmosphere separately at 900 °C for 2 h. The corresponding carbon aerogels were denoted as Fe(Zn)-N-C.

Synthesis of control samples: (1) Mesoporous carbon (CF) was synthesized in parallel by the same method as that for Fe(Zn)-N-C, except for no using $FeCl_3 \cdot 6H_2O$, $Zn(NO_3)_2 \cdot 6H_2O$ and 2-MIM. (2) Fe-N-C was obtained in parallel by the same synthesis route as that for Fe(Zn)-N-C, except for no addition of $Zn(NO_3)_2 \cdot 6H_2O$. (3) (Zn)-N-C was prepared in parallel by the same way as that Fe(Zn)-N-C, except for no applying for $FeCl_3 \cdot 6H_2O$. (4) Fe(Zn)-N-C-*x* (*x*=1, 2, 3), where x indicates the different amount of $FeCl_3 \cdot 6H_2O$ (35, 50 and 65 mg). Unless otherwise specified, Fe(Zn)-N-C refers to the sample prepared at *x*=2 ($FeCl_3 \cdot 6H_2O$, 50 mg).

Microstructural Characterization: The as-prepared samples were examined by transmission electron microscopy (TEM, JEM-2100F, JEOL, Japan) to character the morphologies and the microstructures. X-ray powder diffraction (XRD, D8 Advance, Bruker, Germany) with Cu-K α radiation (λ=1.5406 Å) and Raman spectroscopy (Renishaw inVia, UK Raman spectrometer system) with a laser wavelength of 532 nm investigated to obtain the crystal structure of all samples. The chemical compositions of samples were studied by X-ray photoelectron spectroscopy (XPS, ES-CALAB 250Xi, Thermo Fisher Scientific, America). N_2 sorption isotherms were determined by the Tristar II (Micrometrics, ASAP 2020 HD88) at 77 K. The specific surface area (SSA) was calculated using Brunauer-Emmett-Teller (BET) model. Pore size distribution was analyzed by Barrett-Joyner-Halenda (BJH) model based on the adsorption data.

Electrochemical performance characterization: The ORR electrochemical tests were carried out by using electrochemical workstation (CHI 760E, CH Instruments Inc., Shanghai, China) with a rotating disk electrode (RDE) and rotating ring-disk electrode (RRDE) with a Pt ring in a standard three-electrode cell at room temperature. A graphite rod was employed for counter electrode, glassy carbon (RDE or RRDE) coated with catalytic material as the working electrode and reference electrode of Hg/HgO for tests in 0.1 M KOH and 0.1 M PBS buffer (pH 7.4), reference electrode of Ag/AgCl in 0.5 M H_2SO_4. All recorded potentials are given relative to a reversible hydrogen electrode (RHE) by experimental calibrations: Pt foil was used as both the working electrode and counter electrode, and the electrolyte was saturated with H_2 provided by hydrogen generator. Our result shows that the *E*(Ag/AgCl) is lower than *E*(RHE) by 0.222 V in 0.5 M H_2SO_4, *E*(Hg/HgO) by 0.882 V in 0.1 M KOH and 0.557 V in 0.1 M PBS.

The working electrode was prepared as follows: 4 mg of as-fabricated catalysts was first dispersed in the mixture of deionized water, ethanol and 5% Nafion (6:3:1) by sonication for 30 min in an ice-water bath. Then 5 μl of the ink was dropped on the polished glassy carbon electrode (RDE) to obtain catalysts loading of 0.28 mg cm^{-2} (8.9 μl of the ink for the RRDE)

and dried 1 hour in the air. For comparison, commercial Pt/C (20 wt%) catalyst was also measured with loading of 25 μgpt cm^{-2}.

Before each ORR testing, the system was saturated with O_2 to remove the surface contamination of the catalysts in 0.1 M KOH, 0.5 M H_2SO_4 and 0.1 M PBS solutions, respectively. Cyclic voltammetry (CV) curves were recorded at a scan rate of 20 mV s^{-1} in N_2- or O_2-saturated electrolytes. Linear sweep voltammetry (LSV) was collected at a scan rate of 10 mV s^{-1} at a different rotation speed of 400-2025 rpm. Rotating ring-disk electrode (RRDE) measurements were performed at a rotating speed of 1600 rpm with a scan rate of 10 mV s^{-1} and the ring potential was fixed at 1.4 V versus RHE.

The kinetics parameters were evaluated using the Koutecky-Levich (K-L) equation as follows:

$$\frac{1}{j} = \frac{1}{j_L} + \frac{1}{j_K} = \frac{1}{B\omega^{1/2}} + \frac{1}{j_K} \quad (1)$$

$$B = 0.62\, nFC_0(D_0)^{2/3}\upsilon^{-1/6} \quad (2)$$

where j, j_L and j_K are the measured, diffusion-limiting and kinetic current densities, respectively. ω is the electrode rotation rate in rpm; F is the Faraday constant (F = 96485 C mol^{-1}); C_0 is the bulk concentration of O_2 (1.2×10^{-6} mol cm^{-3}); D_0 is the diffusion coefficient of O_2 (1.9×10^{-5} cm^2 s^{-1}); ν represents the kinematic viscosity of the electrolyte (0.01 cm^2 s^{-1}).

In order to plot the Tafel curves, the kinetic current was calculated from the mass-transport correction of the RDE using:

$$j_K = \frac{j \times j_L}{j_L - j} \quad (3)$$

For RRDEs, the peroxide (H_2O_2) content and the transferred electron number (n) relative to the total products was determined based on the following equations:

$$n = 4 \times \frac{I_D}{\frac{I_R}{N} + I_D} \quad (4)$$

$$H_2O_2(\%) = 200 \times \frac{I_R/N}{\frac{I_R}{N} + I_D} \quad (5)$$

where I_D and I_R represent the disk current and the value of ring current, respectively, and N=0.37 is the current collection efficiency of the Pt ring.

The double layer capacitances were carried out by CV in a potential range from 1.092 V to 1.192 V *vs.* RHE in 0.1 M KOH solution. The scan rates were measured from 10 mV s^{-1} to 100 mV s^{-1}. The C_{dl} can be determined by calculating the half of the slope by plotting the Δj (j_a-j_c) at 1.142 V vs. RHE against the scan rates. Furthermore, electrochemical impedance spectroscopy (EIS) was performed in the frequency range of 0.01 Hz to 1 M Hz in O_2-saturated 0.1 M KOH, 0.5 M H_2SO_4 and 0.1 M PBS solutions, respectively, while perturbation amplitude was set to 5 mV. The durability measurement of the as-prepared catalysts was performed by applying a constant potential at a rotating rate of 1600 rpm.

Liquid Zn-air battery assembly: Zn-air batteries were tested on home-made alkaline/neutral electrochemical cells, where Zn foil as active anode, 6 M KOH was used as the alkaline electrolyte and 4 M NH_4Cl+2 M KCl as the neutral electrolyte. For Pt/C and Fe(Zn)-N-C samples, 5 mg catalyst was ultrasonically dispersed in 1 mL ethanol with 100 μL 5% Nafion to form a homogenous ink. The catalyst ink was then dropped on a cleaned carbon cloth (1.0 mg cm^{-2}), which could be explored as air cathode (without the addition of conductive carbon black). All measurements were carried out on the as-fabricated cell with a CHI760E workstation and LAND multi-channel battery testing system (CT2001A, Wuhan, China) at room temperature.

The specific capacity (C, mAh g^{-1}) was calculated according to the following equation:

$$C = \frac{I\,\Delta t}{m_{Zn}} \qquad (6)$$

where I (mA) represents the current, Δt (h) is the service time and m_{Zn} (g) is the weight of the consumed Zn anode.

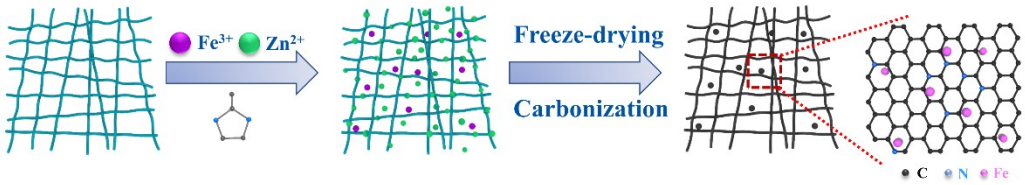

Fig. S1. Schematic illustration for the synthesis of sample Fe(Zn)-N-C.

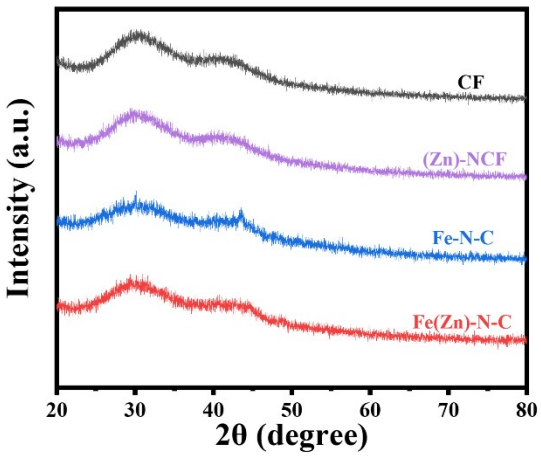

Fig. S2. XRD patterns of samples CF, Fe-N-C, (Zn)-N-C and Fe(Zn)-N-C.

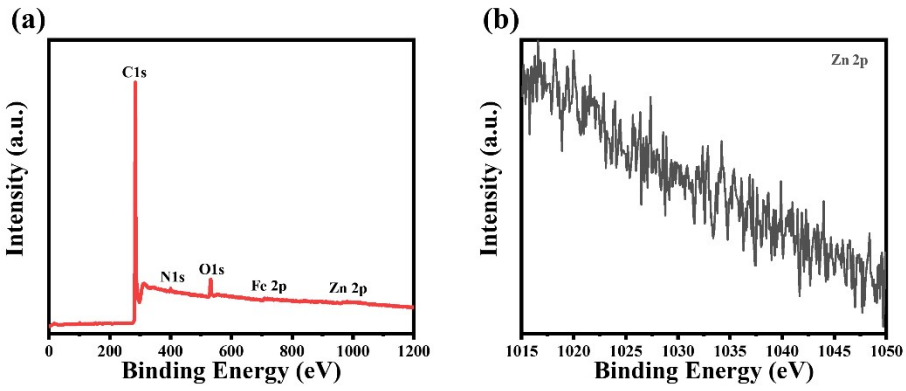

Fig. S3. (a) XPS survey and (b) Zn 2p spectra of Fe(Zn)-N-C catalyst.

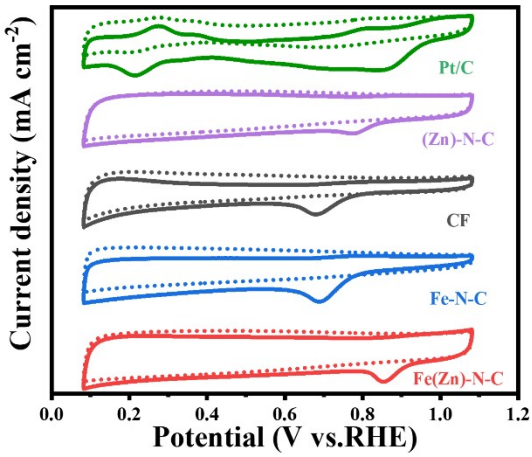

Fig. S4. CV curves of as-prepared catalysts in O_2/N_2-saturated 0.1 M KOH.

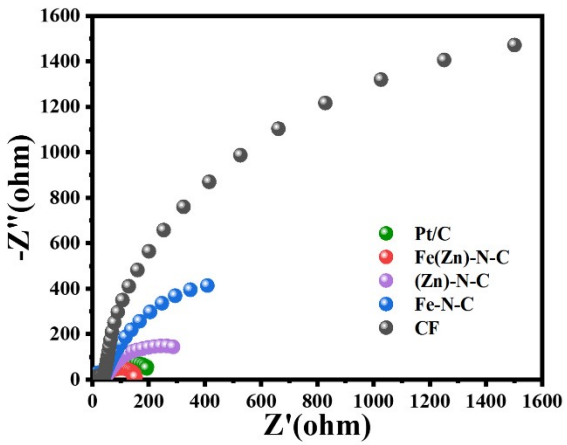

Fig. S5. Nyquist plots of Fe(Zn)-N-C and control samples in O_2 saturated 0.1 M KOH solution.

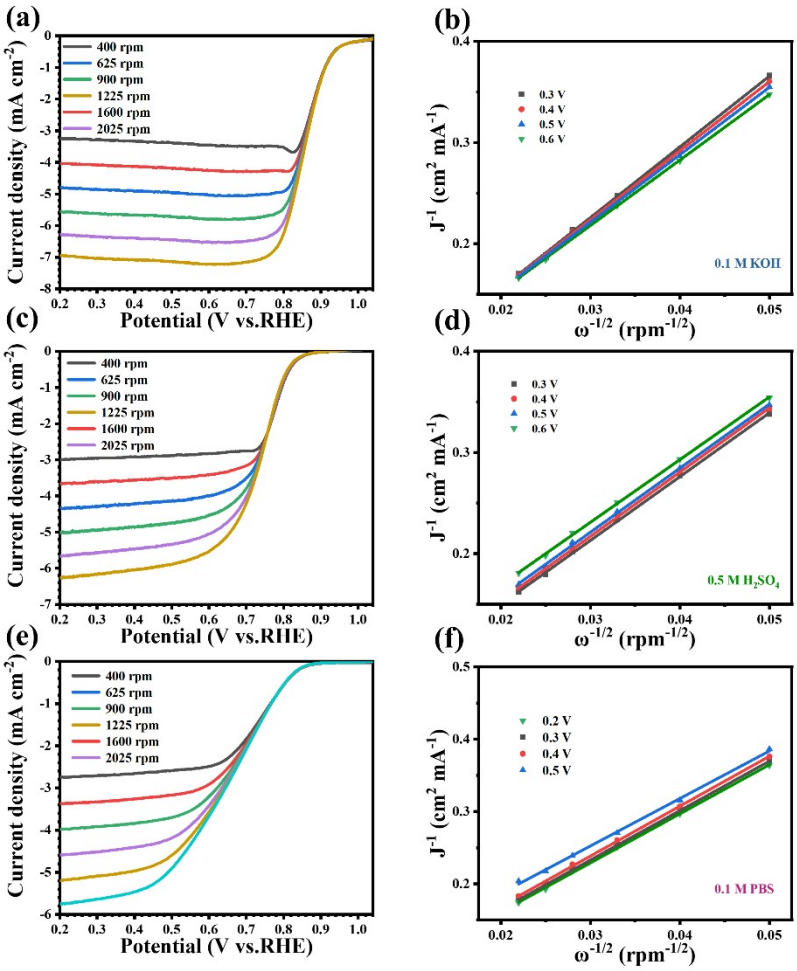

Fig. S6. (a, c, e) LSV curves at different rotating rates and (b, d, e) Koutecky-Levich (K-L) plots of the Fe(Zn)-N-C catalyst in O_2 saturated 0.1 M KOH, 0.5 H_2SO_4 and 0.1 M PBS solutions, respectively.

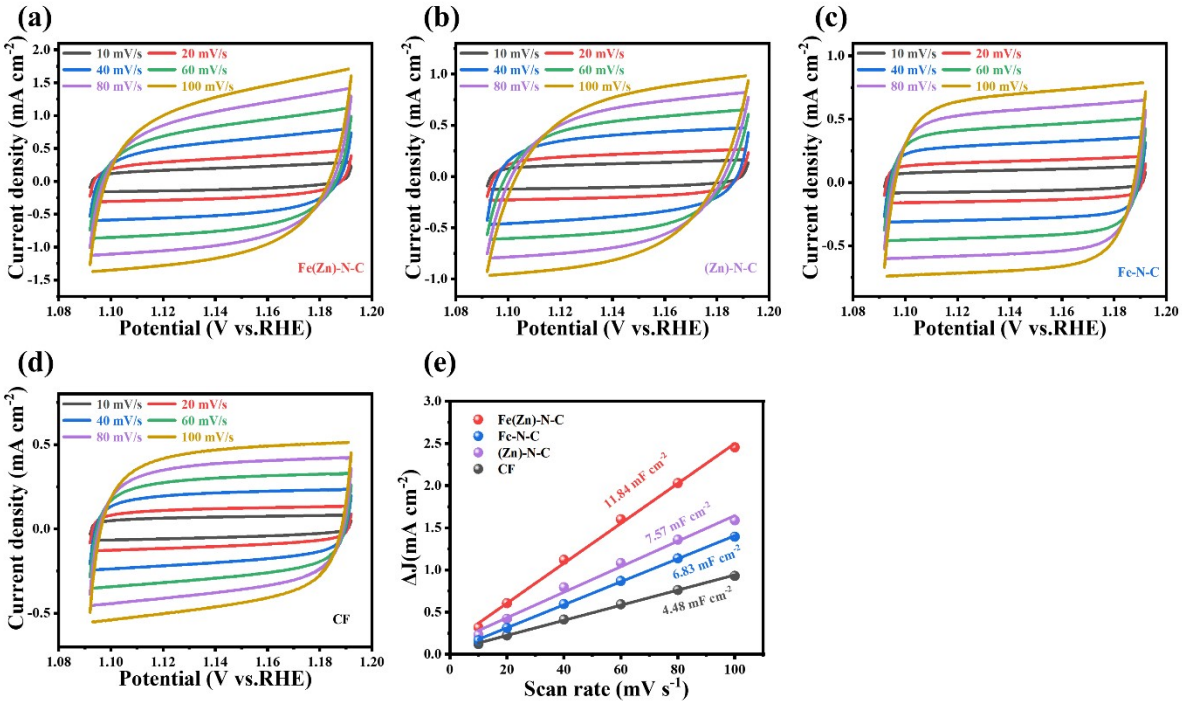

Fig. S7. CV curves of (a) Fe(Zn)-N-C, (b) (Zn)-N-C, (c) Fe-N-C, (d) CF at different scan rate; (e) Current density differences plotted against scan rates of various catalysts.

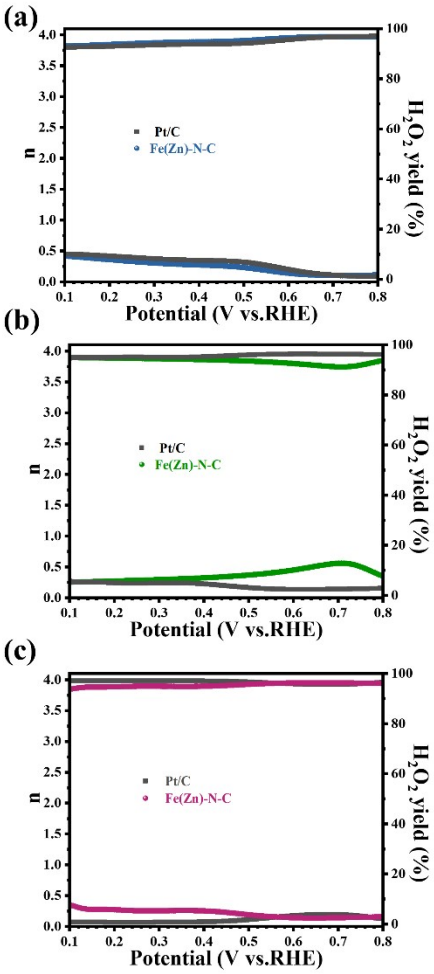

Fig. S8. Electron transfer number and peroxide yield derived from RRDE of the Fe(Zn)-N-C and Pt/C catalysts in O_2 saturated 0.1 M KOH, 0.5 M H_2SO_4 and 0.1 M PBS solutions, respectively.

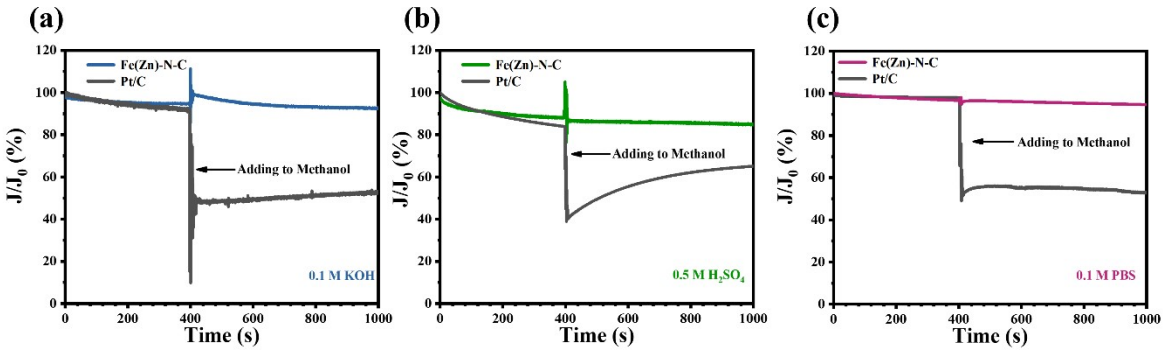

Fig. S9. Chronoamperometric response curves of Fe(Zn)-N-C and Pt/C catalysts before and after the addition of 3 mL methano about 400 s in O_2 saturated 0.1 M KOH, 0.5 M H_2SO_4 and 0.1 M PBS solutions, respectively.

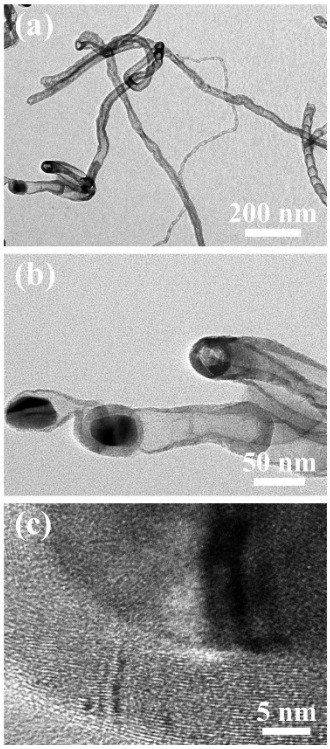

Fig. S10. TEM images of the Fe(Zn)-N-C catalyst after ORR stability test in 0.1 M KOH solution.

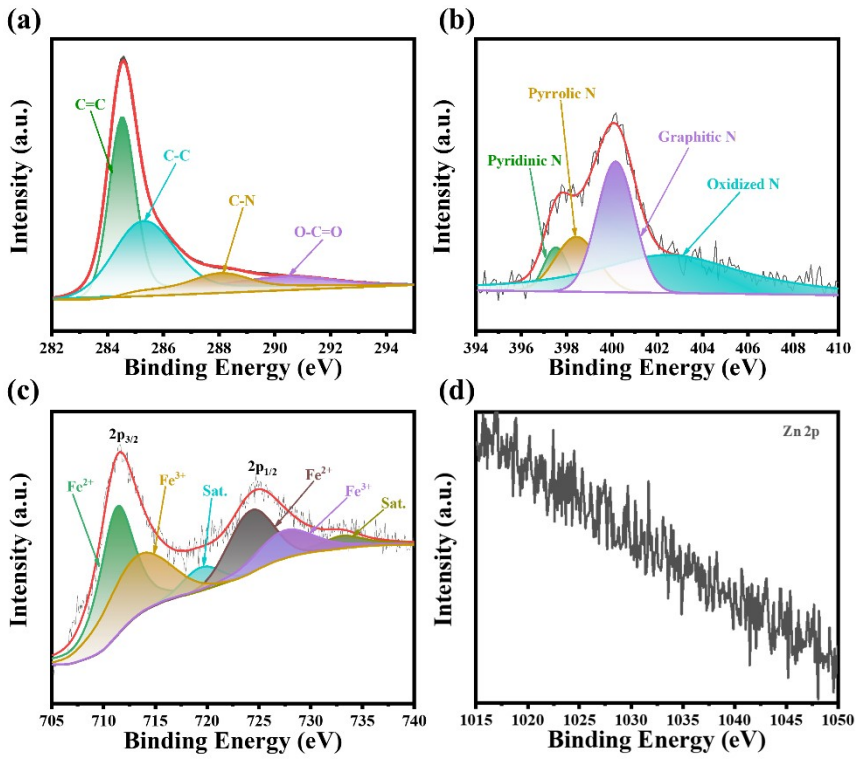

Fig. S11. High-resolution XPS spectra of (a) C 1s, (b) N 1s, (c) Fe 2p and (d) Zn 2p for Fe(Zn)-N-C catalyst after ORR stability test in 0.1 M KOH solution.

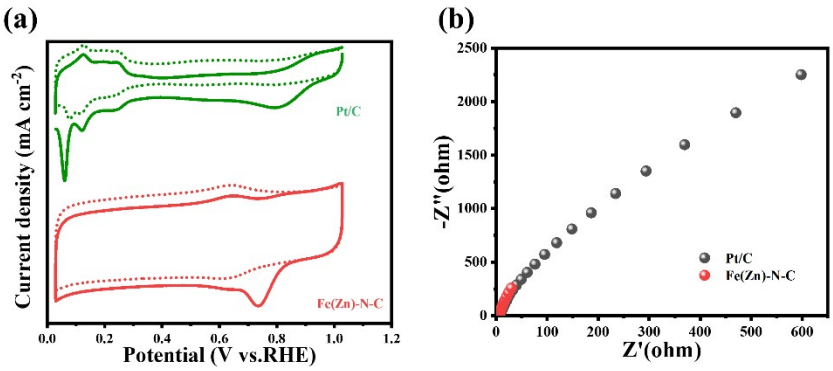

Fig. S12. (a) CV curves, (b) Nyquist plots of Fe(Zn)-N-C and Pt/C catalysts in 0.5 M H_2SO_4 solution.

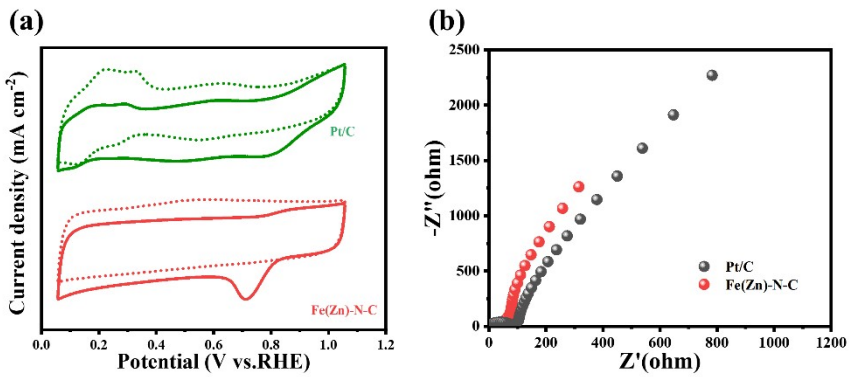

Fig. S13. (a) CV curves, (b) Nyquist plots of Fe(Zn)-N-C and Pt/C catalysts in 0.1 M PBS solution.

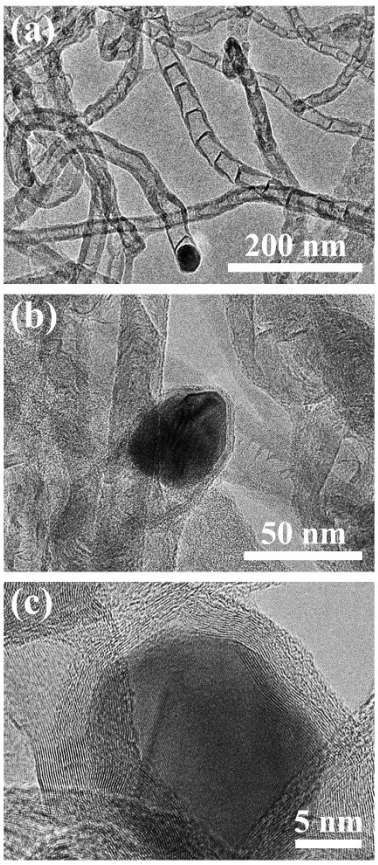

Fig. S14. TEM images of the Fe(Zn)-N-C catalyst after ORR stability test in 0.5 M H_2SO_4 solution.

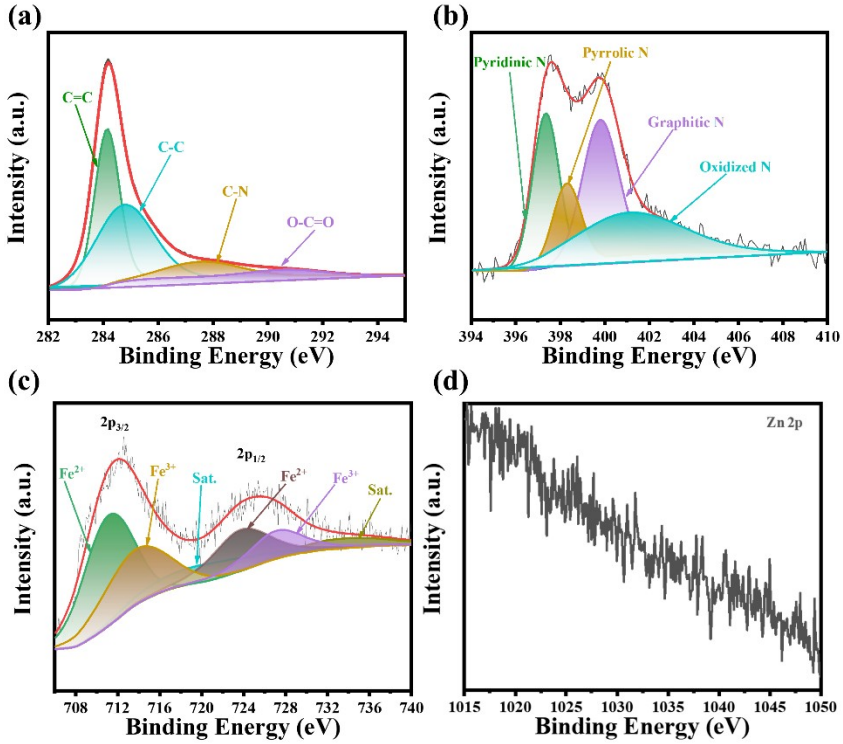

Fig. S15. High-resolution XPS spectra of (a) C 1s, (b) N 1s, (c) Fe 2p and (d) Zn 2p for Fe(Zn)-N-C catalyst after ORR stability test in 0.5 M H_2SO_4 solution.

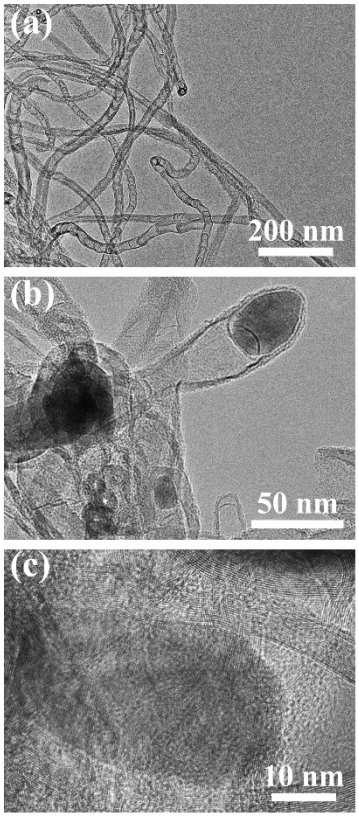

Fig. S16. TEM images of the Fe(Zn)-N-C catalyst after ORR stability test in 0.1 M PBS solution.

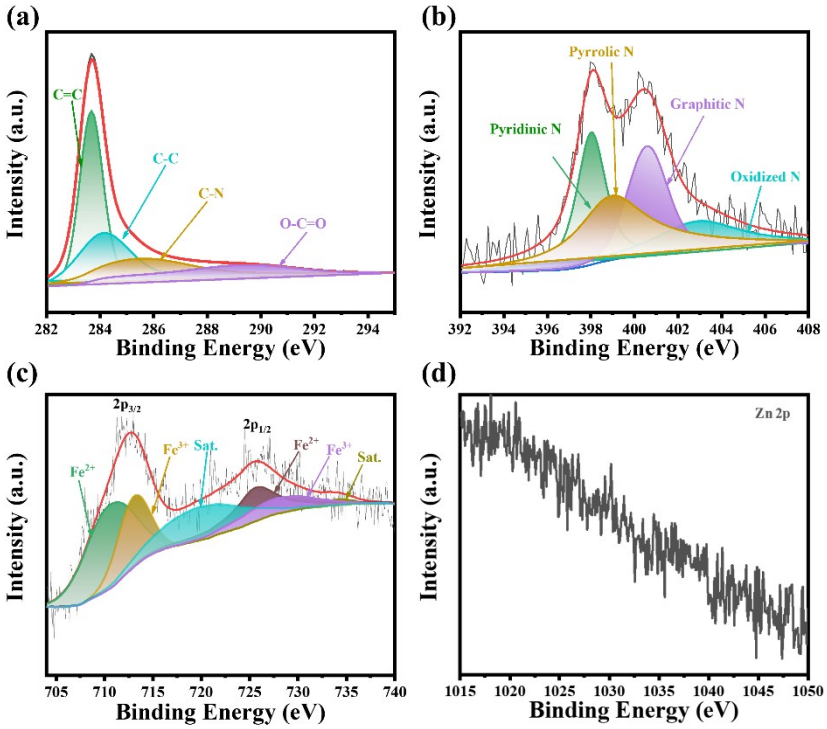

Fig. S17. High-resolution XPS spectra of (a) C 1s, (b) N 1s, (c) Fe 2p and (d) Zn 2p for Fe(Zn)-N-C catalyst after ORR stability test in 0.1 M PBS solution.

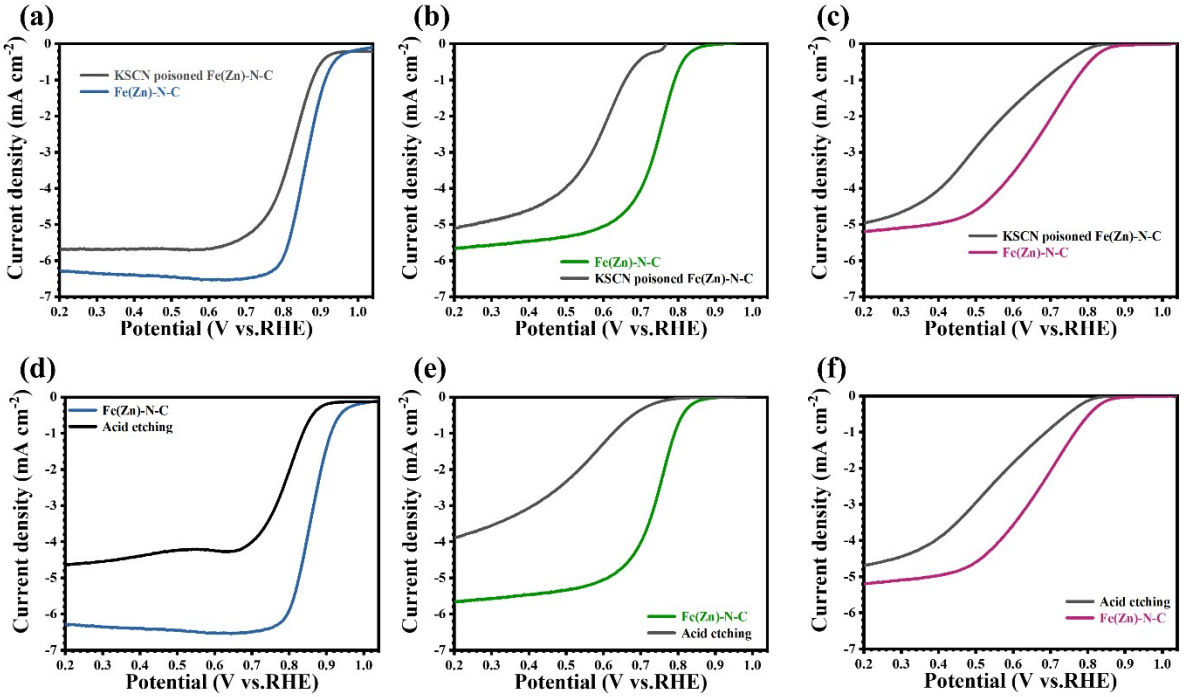

Fig. S18. (a-c) ORR polarization curves of Fe(Zn)-N-C and Pt/C catalysts with or without 10 mM KSCN, (d-f) before and after hot acid etching in O_2-saturated 0.1 M KOH, 0.5 M H_2SO_4 and 0.1 M PBS solutions, respectively.

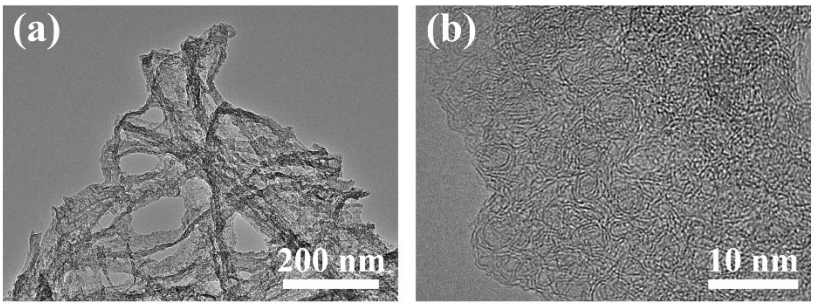

Fig. S19. TEM images of Fe(Zn)-N-C treated by hot acid etching.

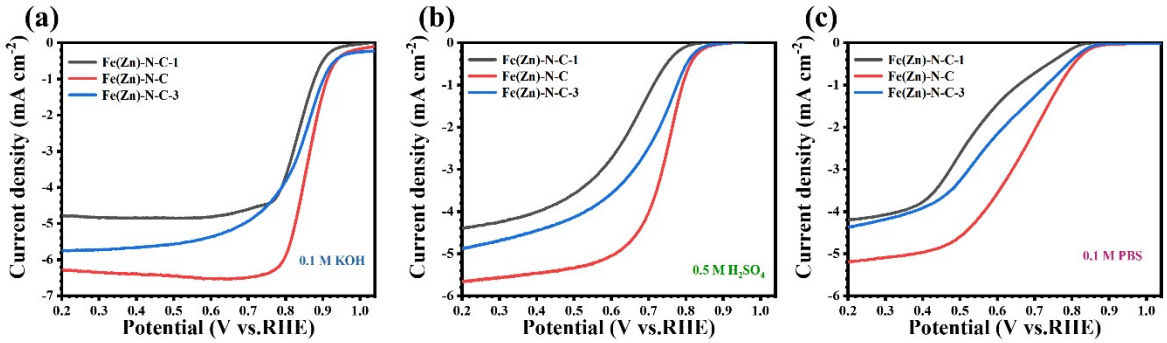

Fig. S20. LSV curves of ORR for the Fe catalysts pyrolyzed from the precursors of different Fe concentrations ($FeCl_3 \cdot 6H_2O$ concentration: 35, 50 and 65 mg) at a rotating rate of 1600 rpm in O_2-saturated 0.1 M KOH, 0.5 M H_2SO_4 and 0.1 M PBS solutions, respectively.

Table S1. The ORR performance of CF, (Zn)-N-C, Fe-N-C, Fe(Zn)-N-C and Pt/C catalysts in O_2-saturated 0.1 M KOH, 0.5 M H_2SO_4 and 0.1 M PBS solutions.

Catalysts	$E_{1/2}$ (V vs. RHE)	Limiting current density (mA cm^{-2})	Tafel slop (mV dec^{-1})	Current retention after 86400 s chronoampero metric test (%)	Electrolyte
CF	0.62	3.02	100	-	0.1 M KOH
(Zn)-N-C	0.76	4.51	80	-	
Fe-N-C	0.65	4.21	94	-	
Fe(Zn)-N-C	**0.86**	**6.16**	**66**	**85**	
Pt/C	0.82	5.68	75	63	
Fe(Zn)-N-C	**0.74**	**5.81**	**61**	**80**	0.5 M H_2SO_4
Pt/C	0.78	4.74	91	48	
Fe(Zn)-N-C	**0.67**	**5.26**	**76**	**82**	0.1 M PBS
Pt/C	0.61	4.65	131	56	

Table S2. Comparison of ORR performance of Fe(Zn)-N-C catalyst with non-precious electrocatalysts in 0.1 M KOH.

Catalysts	$E_{1/2}$ (V vs. RHE)	Tafel slop (mV dec^{-1})	Stability	Ref.
Fe/Fe_3C@C	0.831	87	94% retention after 20,000s	2
Fe-N-C/Fe_3C-op	0.911	83.4	95% retention after 43,200s	3
SA-Ir/NC	0.84	65.1	$E_{1/2}$ of 10 mV shift after 20,000 cycles	4
NC@Co-HPNC	0.83	87.63	$E_{1/2}$ of 5 mV shift after 2,000 cycles	5
FeNPC	0.904	84	92.2% retention after 36,000s	6
Fe_H-N-C	0.91	58	$E_{1/2}$ of 29 mV shift after 100,000 cycles	7
CuCo-NC/NPs	0.87	64.3	93% retention after 72,000s	8
Fe SA/NCZ	0.87	70	$E_{1/2}$ of 10 mV shift after 10,000 cycles	9
$Fe_{0.5}Co$@HOMNCP	0.903	82	96.4% retention after 36,000s	10
Fe(Zn)-N-C	**0.86**	**66**	**85% retention after 86,400s**	**This work**

Table S3. Comparison of ORR performance of Fe(Zn)-N-C catalyst with non-precious electrocatalysts in acidic media.

Catalysts	Electrolyte	$E_{1/2}$ (V vs. RHE)	Tafel slop (mV dec^{-1})	Stability	Ref.
Fe-pyridinic N-C	0.1 M $HClO_4$	0.825	63.8	83.4% retention after 28,800s	11
PNC-30	0.1 M $HClO_4$	0.76	65	93.2% retention after 20,000s	12
H-S-Fe-NC	0.1 M $HClO_4$	0.782	-	91.8% retention after 36,000s	13
Co_xFe_y@N-C	0.5 M H_2SO4	0.83	97	$E_{1/2}$ of 18 mV shift after 5,000 cycles	14
Fe/Ni-N-PCS	0.1 M $HClO_4$	0.71	126	-	15
Fe@MNC-OAc	0.1 M $HClO_4$	0.838	70.4	96.27% retention after 15,000s	16
Fe_1NGF	0.1 M $HClO_4$	0.813	74	Slight shift of $E_{1/2}$ after 5,000 cycles	17
Mn-Fe@NCNTs	0.1 M $HClO_4$	0.76	78.5	90.1% retention after 29,000s	18
D-MN4-CNF-IL-A	0.5 M H_2SO4	0.71	61	~86% retention after 43,200s	19
Fe(Zn)-N-C	**0.5 M H_2SO4**	**0.74**	**61**	**80% retention after 86,400s**	**This work**

Table S4. Comparison of ORR performance of Fe(Zn)-N-C catalyst with non-precious electrocatalysts in neutral media.

Catalysts	$E_{1/2}$ (V vs. RHE)	Tafel slop (mV dec^{-1})	Stability	Ref.
$NiFe_2O_4/FeNi_2S_4$ HNSs	0.507	-	almost no decay after 5,000 cycles	20
Fe-N-C/800-HT2	0.743	91	89.4% retention after 28,800s	21
G/C-Fe-2	-	-	78.7% retention after 10,000s	22
FePc@CTS	0.057V vs. Ag/AgCl	51.3	-	23
eFe-N_3/PCF	0.72	-	89.9% retention after 10,000s	24
Fe_xN/NC-7	0.80	-	-	25
Fe SAs/NC	0.75	67.4	-	26
5%Fe-N/C	0.64	-	-	27
Fe(Zn)-N-C	**0.61**	**76**	**82% retention after 86,400s**	**This work**

Table S5. Comparison of $E_{1/2}$ of Fe(Zn)-N-C catalyst with pH-universal non-precious electrocatalysts in alkaline, acidic and neutral media.

Catalysts	Alkaline $E_{1/2}$ (V vs. RHE)	Acidic $E_{1/2}$ (V vs. RHE)	Neutral $E_{1/2}$ (V vs. RHE)	Ref.
CeNCs	0.9	0.83	0.78	28
γ-Fe_2O_3@CNFs-12	0.905	0.693	0.58	29
FeSA/PNC	0.92	0.84	0.83	30
Fe/Fe_3C/NHCS	0.84	0.67	0.71	31
MFS-Fe-0.7	0.83	0.64	0.76	32
Fe–N/C	0.823	0.661	positive than Pt/C catalyst	33
Fe/NC-3	0.90 (1 M KOH)	0.71	0.69	34
Fe-Zn-SA/NC	0.85	0.78	0.72	35
Fe-NX@NSCST-ZL	0.94	0.77	0.74	36
Fe(Zn)-N-C	**0.86**	**0.74**	**0.61**	**This work**

Table S6. Comparison of reported alkaline/neutral liquid Zn-air batteries based on well-developed non-precious oxygen catalysts .

Catalysts	Electrolyte	Power Density (mW cm^{-2})	Specific capacity@10 mA cm^{-2} (mAh g^{-1})	Ref.
Fe_1/d-CN	6 M KOH +0.2 M $Zn(Ac)_2$	144	770	37
	4 M NH_4Cl+2 M KCl	34	653	
Fc@Fe–NHCS	6 M KOH	196	769@100 mA cm^{-2}	38
	4 M NH_4Cl+1 M KCl	58	-	
Fe-NBrGo	6 M KOH+0.15 M ZnO	107	-	39
	4 M NH_4Cl+2 M KCl	34	-	
NHCS@B_1P_2	6 M KOH	158.5	-	40
	4 M NH_4Cl+1 M KCl	104.6	-	
Fe-NC@NHCS-600	6 M KOH	278.97	-	41
	4 M NH_4Cl+1 M KCl	114.96	-	
FeCo SAs@Co/N-GC	6 M KOH	207	741@5 mA cm^{-2}	42
	3 M $Zn(TFSI)_2$	162	813@2 mA cm^{-2}	
SA-Ir/NC	0.1 M PBS+ 0.02 M $Zn(CH_3COO)_2$	76	776.8 @20 mA cm^{-2}	4
Fe(Zn)-N-C	**6 M KOH**	**193**	**800**	**This work**
	4 M NH_4Cl+2 M KCl	**48**	**688**	

Reference

1. Y. Ma, D. Chen, Z. Fang, Y. Zheng, W. Li, S. Xu, X. Lu, G. Shao, Q. Liu and W. Yang, Proc. Natl. Acad. Sc.i U. S. A., 2021, **118**, e2105610118.
2. W. Dong, T. Wang, W. Yang, K. Song and Z. Zou, Electrochem. Commun., 2023, **150**, 107477.
3. J. Chang, Q. Zhang, J. Yu, W. Jing, S. Wang, G. Yin, G. I. N. Waterhouse and S. Lu, Adv. Sci., 2023, **10**, 2301656.
4. X. Luo, M. Yang, W. Song, Q. Fang, X. Wei, L. Jiao, W. Xu, Y. Kang, H. Wang, N. Wu, W. Gu, L. Zheng, L. Hu and C. Zhu, Adv. Funct. Mater., 2021, **31**, 2101193.
5. Z. Chi, Y. Feng, Y. Ma, D. Kong, H. Yin, S. Li, L. Li, Z. Guo and L. Wang, Chem. Commun. (Camb), 2021, **57**, 11248-11251.
6. L. Fan, X. Wei, X. Li, Z. Liu, M. Li, S. Liu, Z. Kang, F. Dai, X. Lu and D. Sun, Nano Research, 2022, **16**, 1810-1819.
7. H. Tian, A. Song, P. Zhang, K. Sun, J. Wang, B. Sun, Q. Fan, G. Shao, C. Chen, H. Liu, Y. Li and G. Wang, Adv. Mater., 2023, **35**, e2210714.
8. J. Feng, D. Zheng, R. Yin, X. Niu, X. Xu, S. Meng, S. Ma, W. Shi, F. Wu, W. Liu and X. Cao, Small Struct., 2023, **4**, 2200340.
9. C. Jiao, Z. Xu, J. Shao, Y. Xia, J. Tseng, G. Ren, N. Zhang, P. Liu, C. Liu, G. Li, S. Chen, S. Chen and H. L. Wang, Adv. Funct. Mater., 2023, **33**, 2213897.
10. W. Li, B. Liu, D. Liu, P. Guo, J. Liu, R. Wang, Y. Guo, X. Tu, H. Pan, D. Sun, F. Fang and R. Wu, Adv. Mater., 2022, **34**, e2109605.
11. L. Li, Y. Wen, G. Han, Y. Liu, Y. Song, W. Zhang, J. Sun, L. Du, F. Kong, Y. Ma, Y. Gao, J. Wang, C. Du and G. Yin, Chem. Eng. J., 2022, **437**, 135320.
12. B. Liu, F. Liu, D. Lu, S. Zhang, C. Zhang, Z. Gao, L. Shi, Y. Liu, J. X Shi, L. Zhang, S. Zhao and D. Liu, Chem. Eng. J., 2022, **430**, 132762.
13. J. Yan, T. Gu, R. Shi, X. Chen, M. H. Rümmeli and R. Yang, J. Mater. Chem. A, 2023, **11**, 16180-16189.
14. J. Liu, Z. P. Li and B. H. Liu, J. Alloy. Compd., 2023, **944**, 169166.
15. J. Zhao, L. Zong, L. Cui, F. Lu, Z. Xiao and L. Wang, J. Colloid Interface Sci., 2023, **633**, 828-835.
16. Y. Liu, F. Tu, Z. Zhang, Z. Zhao, P. Guo, L. Shen, Y. Zhang, L. Zhao, G. Shao and Z. Wang, Appl. Catal. B-Environ., 2023, **324**, 122209.
17. F. Li, G.-F. Han, W. Che, J.-M. Seo, W. Zou, H. Liu, I. Ahmad, Z. Fu, Y. Lu and J.-B. Baek, Nano Energy, 2023, **114**, 108647.
18. X. Guo, S. Xue, X. Zhang, J. Qin, M. Hong, Q. Chen, W. Liu, C. Du and J. Chen, J. Alloy. Compd., 2023, **953**, 169992.
19. K. Muuli, M. Mooste, S. Akula, V. Gudkova, M. Otsus, A. Kikas, J. Aruväli, A. Treshchalov, V. Kisand, A. Tamm, A. Krumme, S. Cavaliere and K. Tammeveski, ChemElectroChem, 2023, **10**, e202300131.
20. L. An, Z. Zhang, J. Feng, F. Lv, Y. Li, R. Wang, M. Lu, R. B. Gupta, P. Xi and S. Zhang, J. Am. Chem. Soc., 2018, **140**, 17624-17631.
21. G. Zhang, L. Li, M. Chen and F. Yang, J. Mater. Chem. A, 2020, **8**, 9256-9267.
22. H. Wang, L. Wei and J. Shen, Int. J. Hydrogen Energy, 2022, **47**, 17982-17991.
23. Y. Zhang, J. Li, W. Yang, J. Zhang, Q. Fu, Y.-C. Song, Z. Wei, Q. Liao and X. Zhu, Electrochim. Acta, 2020, **363**, 137177.
24. J. Liu, Z. Gong, C. Allen, W. Ge, H. Gong, J. Liao, J. Liu, K. Huang, M. Yan, R. Liu, G. He, J. Dong, G. Ye and H. Fei, Chem Catalysis, 2021, **1**, 1291-1307.
25. X. Hu, Y. Min, L. L. Ma, J. Y. Lu, H.C. Li, W.J. Liu, J.J. Chen and H.Q. Yu, Appl. Catal.

B-Environ., 2020, **268**, 118405.
26. Z. Li, S. Ji, C. Xu, L. Leng, H. Liu, J. H. Horton, L. Du, J. Gao, C. He, X. Qi, Q. Xu and J. Zhu, Adv. Mater., 2023, **35**, 2209644.
27. L.Q. Yu, H. Wang, S.L. Chen, T.E. Wen, B.C. Huang and R.C. Jin, Chinese Chem. Lett., 2023, **34**, 107236.
28. Y. Zhao, H. Wang, J. Li, Y. Fang, Y. Kang, T. Zhao and C. Zhao, Adv. Funct. Mater., 2023, 2305268.
29. Z. Yao, Y. Li, D. Chen, Y. Zhang, X. Bao, J. Wang and Q. Zhong, Chem. Eng. J., 2021, **415**, 129033.
30. W. Xue, Q. Zhou, X. Cui, J. Zhang, S. Zuo, F. Mo, J. Jiang, X. Zhu and Z. Lin, Angew Chem. Int. Ed. Engl., 2023, **62**, e202307504.
31. Y. Liu, X. Wang, B. Zhao, X. Shao and M. Huang, Chem.- Eur. J., 2019, **25**, 9650-9657.
32. F. Zhang, Y. Chen, Y. Liu, X. Liu and S. Gao, Int. J. Hydrogen Energ., 2021, **46**, 37895-37906.
33. X. Luo, W. Han, W. Du, Z. Huang, Y. Jiang and Y. Zhang, J. Power Sources, 2020, **469**, 228184
34. M. Liu, J. Lee, T. C. Yang, F. Zheng, J. Zhao, C. M. Yang and L. Y. S. Lee, Small Methods, 2021, **5**, e2001165.
35. J. Xu, S. Lai, D. Qi, M. Hu, X. Peng, Y. Liu, W. Liu, G. Hu, H. Xu, F. Li, C. Li, J. He, L. Zhuo, J. Sun, Y. Qiu, S. Zhang, J. Luo and X. Liu, Nano Research, 2020, **14**, 1374-1381.
36. C. Li, Y. Zhang, M. Yuan, Y. Liu, H. Lan, Z. Li, K. Liu and L. Wang, Chem. Eng. J., 2023, **471**, 144515.
37. M. Zhao, H. Liu, H. Zhang, W. Chen, H. Sun, Z. Wang, B. Zhang, L. Song, Y. Yang, C. Ma, Y. Han and W. Huang, Energy Environ. Sci., 2021, **14**, 6455-6463.
38. K. Sheng, J. Li, G. Li, J. Hao, Y. Wang, Y. Liu, Y. Liu, Q. Yi and W. Li, Appl. Surf. Sci., 2022, **601**, 154221.
39. Y. Irmawati, F. Balqis, P. B. Persada, F. Destyorini, R. Yudianti, F. Iskandar and A. Sumboja, Batteries, 2023, **9**, 356.
40. Y. Wang, A. Chen, C. Fang and Q. Yi, Ind. Eng. Chem. Res., 2022, **61**, 10969-10981.
41. Y. Wang, R. Yi, A. Chen, C. Fang, Y. Wang, Q. Yi, M. Liu, S. Liu, S. Zhan and B. Zhong, Energy Technol., 2022, **10**, 2200057.
42. N. K. Wagh, D. H. Kim, S. H. Kim, S. S. Shinde and J. H. Lee, ACS Nano, 2021, **15**, 14683-14696.